JOURNAL OF MATERIALS SCIENCE 17(1982) 595–606

The processing and static mechanical properties of metal fibre reinforced bioglass

P. DUCHEYNE
Katholieke Universiteit Leuven, Leuven, Belgium

L.L. HENCH
University of Florida, Gainesville, Florida, USA

The development of bioglass composites is presented. Stainless steel AISI 316 L fibres are introduced into bioglass by immersion of premade porous fibre skeletons into molten bioglass. It is shown that this technique is simple and effective in obtaining metal fibre reinforced bioglass. Thermal shock, tensile tests and three-point bend tests all show a marked increase of strength of the composite over the parent glass and a substantial improvement of toughness.

1. Introduction

Few materials can presently be used for temporary and permanent medical and dental implants, especially when the implant is subjected to high stresses. They include AISI 316 L stainless steel, cast, wrought or hot isostatically pressed cobalt–chromium–molybdenum alloys, wrought cobalt–chromium–nickel alloys, commercially pure titanium, Ti–6 wt % Al–4 wt % V alloys, high density polyethylene, dense alumina and carbon. Because these materials cause the formation of a fibrous capsule which can result in loosening of the implant, efforts have been made to develop new materials which chemically bond to tissues. There is now considerable evidence that surface active bioglasses form a bond with osseous tissue [1–3] under appropriate conditions. Recent studies also show some evidence of soft tissue adherance to bioglasses [4, 5]. However, disadvantages of bioglasses are their limited strength and poor ductility. Therefore present applications are in form of coatings on either dense alumina [6] or metal [7].

The present work describes a new approach to mechanically improving bioglass products. Ductile metal fibres are introduced into the glass to produce a metal fibre reinforced bioglass composite. The metal fibres improve both strength and deformability. They also result in a composite material with elastic properties more closely matching the elasticity of the surrounding bone than metallic alloys; this reduces the risk of bone resorption.

The most widely used technique for the fabrication of fibre reinforced ceramics and glasses is hot pressing. Other techniques have been listed by Donald and McMillan [8] in their review on ceramic matrix composites including: cold-pressing and sintering, slip casting and sintering, plasma-spraying, casting of certain glass–alumina fibre systems, extrusion and uni-directional solidification of ceramic–metal eutectic structures.

In this study a new method for producing composites is described which involves immersing a preformed metal fibre skeleton in the molten glass batch. The aims of the present paper are (a) to describe the materials and processing variables associated with this novel technology for producing glass–fibre composites, and (b) to report the considerable improvement of mechanical properties as a result of loading the glass matrix with a ductile second phase.

2. General method for preparation of the composites

In all experiments the composites were made of 45-S-5 bioglass [1, 2] and AISI 316 L stainless steel fibres. The nominal composition of this type of

0022–2461/82/020595–12$3.20/0

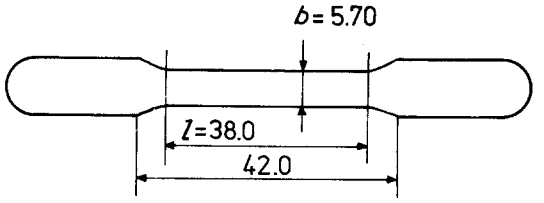

Figure 1 Mechanical test specimens before and after immersion.

bioglass is: 45 wt % Sio_2, 24.5 wt % CaO, 24.5 wt % Na_2O and 6 wt % P_2O_5. AISI 316 L stainless steel has the following compositional brackets for the more important alloying elements: 17 to 20 wt % Cr, 10 to 14 wt % Ni, 2 to 4 wt % Mo, < 0.03 wt % C. The preparation of the composites involves a number of steps which were optimized in the present work. The sequence is typically as follows: the exact amount of fibres for a given geometry are weighed and compacted under pressure, the fibres are sintered at 1250° C and then the density of the preform is inspected using radiography. The surface of the sintered metal fibre preform is oxidized for 10 min in air at 800° C. The total metal shrinkage is controlled by holding the porous preform at 400° C for 20 min, and then it is immersed into molten glass maintained at 1350 to 1380° C, and finally the glass impregnated preform is annealed at 400 to 500° C for 4 hours and furnace cooled.

3. Preliminary thermal shock testing

In order to test potential improvements in the mechanical properties of the metal fibre reinforced glass composites several thermal shock experiments were performed.

Composite specimens with a 42/58 volume ratio of fibre to glass were prepared using 100 μm diameter fibres 4 mm long. Dimensions of the compacts were as represented in Fig. 1, but sawn in half. A processing procedure similar to that described in Section 2 was followed except for the following. After immersion into glass 45-S-5 at 1375° C, the composites were subjected to a 3 h nucleation at 500° C and a 3 or 6 h crystallization treatment at 800° C. The purpose for crystallizing the composite was to achieve a more direct comparison with previous thermal shock tests of partially crystallized bioglass coatings on stainless steel rods [9]. The thermal shock specimens were subjected to increasing temperature differences in steps of 25° C, followed by an immediate plunge into water at room temperature until fracture occurred.

Since temperature differences during thermal shocking are, within certain assumptions [10], proportional to the stresses developed at the glass–metal interface, an increase in maximum temperature to induce fracture should indicate potential strengthening of the glass by the metal fibres. Previous studies showed that the maximum temperature shock the 0.3 mm bioglass coating could withstand was 325° C. Failure occurred at about 100 μm from the glass–metal interface. The AISI 136 L stainless steel fibre–45-S-5 bioglass composite with an outer rim of 0.3 to 0.5 mm thick unreinforced glass could withstand much greater temperature differences, i.e., 425° C for specimens crystallized for 3 hours, 450° C for specimens crystallized for six hours.

Cracking was observed only in the outer glass rim of the composites. Cracks did not penetrate into the glass matrix of the composite, even though the fibre preform structure was not optimized. Fig. 2 shows that the cracks were parallel with the composite surface with an undamaged internal structure after the 450° C thermal shock. Thus, the preliminary tests indicated that metal fibre reinforcement enhances the mechanical properties of the bioglass, both as the matrix phase of a composite and also as the thin rim of a composite substrate. Based upon these positive findings, a detailed study was conducted to determine the effects of the microstructure of the fibre preform, and the effects of the processing variables on the mechanical properties of the fibre reinforced bioglass composites.

4. Mechanical test procedure

Optimization of the fibre preform microstructure and the composite processing variables was based upon changes in tensile strength and three-point bend strength.

Tensile testing was performed in air with an initial cross-head speed of 0.2 mm min^{-1}. The specimen configuration and dimensions are given in Fig. 1. The thickness was 1.8 mm ± 10 %. At the 0.2 % yield stress the specimen was unloaded. Subsequently it was loaded until fracture at a cross-head speed of 0.5 mm min^{-1}. An extensometer with a 10 mm span and 10 % range was used throughout. Specimens tested in the three point bending mode had a 3 cm span between supports and a cross-head speed of 0.5 mm min^{-1}.

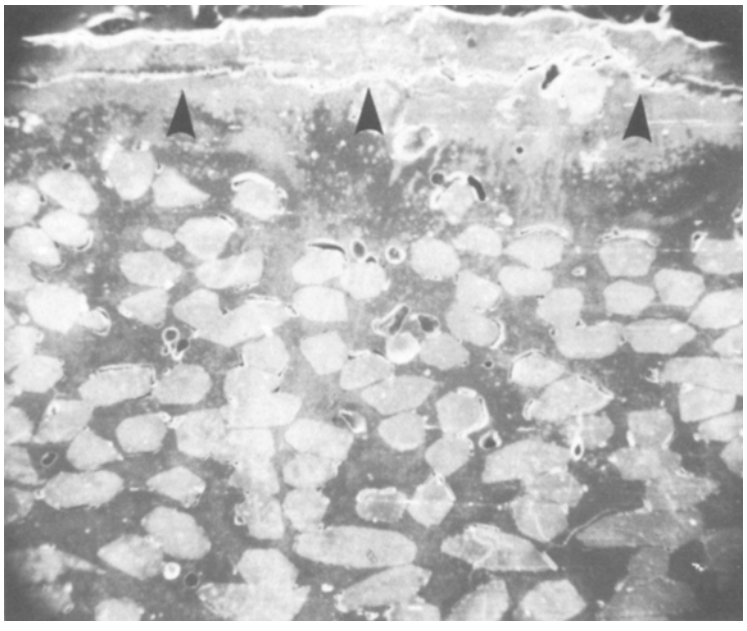

Figure 2 Cross-sectional micrograph of a specimen subjected to thermal shock testing; note the cracking parallel with the composite; no cracking is observed within the composite.

Fig. 3 shows a typical graph recorded from a tensile test of the composite. Because of the observed ductile behaviour of the composite the practice of tensile testing of metals was followed and $\sigma_{0.01}$ and $\sigma_{0.2}$ values were selected from the graphs as characteristics of the material. This was possible by the use of an extensometer to record permanent deformation.

Fig. 3 shows that, within the extensometer span, plastic deformation is clearly present. Upon unloading and reloading, a permanent deformation is recorded. However, the elongation to fracture, measured by the extonsometer, can differ from the actual deformation since fracture onset and plastic tearing of the composite does not always occur within the extensometer span. Approximately 10% of the specimens failed at the transition between the gauge and the shoulder rather than in the extensometer span.

Three-point bend tests were carried on until a deformation of 90° bend angle was reached, the maximum obtainable with the experimental set-up used. Thus the bend strengths reported are generally the stress required to bend the sample 90° rather than the fracture strengths.

5. Composite fabrication variables

5.1. Preform microstructure

Three variables were investigated in establishing an optimal fibre preform compact: sintering of the

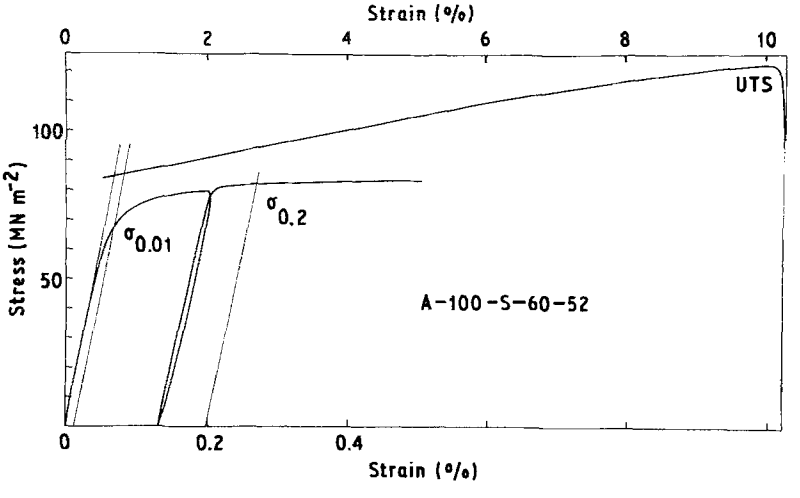

Figure 3 Tensile graph of a 100-S-60 specimen, showing plastic deformation in excess of 10%.

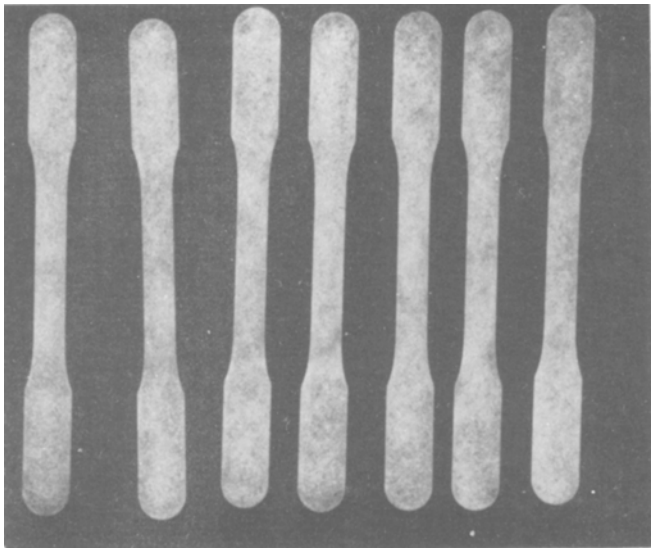

Figure 4 Radiograph of a series of 7 fibre skeletons prior to immersion showing overall microstructural homogeneity (specimens made of 60 vol% 100 μm fibres).

preform fibres, the degree of cold-work of the fibres, and the fibre diameter.

It was found that sintering of the porous compacts was essential for subsequent glass impregnation to be effective. Unsintered compacts of all three fibre diameters studied (50, 100 and 200 μm) were never filled with glass except for a thin $\sim$ 0.1 mm thick surface layer.

Cold worked fibres also were not suitable. They were difficult to compact because of the high elastic spring-back of the wires within the green compact. After pressing, the porous skeletons were fragile and were very difficult to handle. Moreover, cold worked fibre compacts could not be sintered without eliminating the strengthening effect of cold working.

Using constant 4 mm length fibres, it was found that compaction of 45 vol% fibres did not yield a coherent compact with 200 μm diameter fibres. However, compaction and handling of the 50 and 100 μm diameter fibres was possible even at 45 vol% fibres without any major difficulties. Compaction of all fibre types at 60 vol% of fibres could be performed smoothly.

The uniformity of the density of the porous sintered and unsintered skeletons was checked radiographically. Compacts made with 100 and 200 μm fibres had a homogeneous density. The flowability of 50 μm fibres was, however, considerably lower which occasionally resulted in non-uniform filling of the die and non-uniform density after the subsequent compaction. Fig. 4 shows the radiograph of a series of 7 specimens made with 60 vol% of 100 μm fibres. Filling the mould mechanically instead of manually, as was done in these laboratory scale experiments, would probably eliminate any inhomogeneities.

5.2. Variables affecting glass impregnation

Previous studies of the coating of dense stainless steel or Vitallium® rods by immersion dipping showed that the quality of the coating depended on (a) viscosity of the molten glass, (b) thermal expansion of the metal substrate and glass, (c) oxidation and roughness of the metal surface, (d) metal temperature at time of immersion, (e) length of immersion and (f) time and temperature of annealing of the coating. It was recognized that in addition to optimizing these six variables in the immersion process for impregnating the porous metal structure both the volume-fraction and size of porosity would be major processing variables as well. Because of mismatch between the thermal expansion coefficients of glass matrix and the sintered fibre structure, there is also considerable potential for developing internal stresses during the cooling of the composite.

Depending upon whether there is a positive or negative value for the mismatch between thermal expansion coefficients of glass and fibre, the residual stresses generated in the matrix will be either tensile or comprehensive.

The mismatch can be evaluated in a convenient manner by using the linear thermal expansion coefficient, α, where

$$\Delta \alpha_c = \alpha_g - \alpha_f, \quad (1)$$

with the subscripts c meaning composite, g meaning glass matrix and f meaning metal fibre.

The value of α for stainless steel is $16.2 \times 10^{-6}\,^{\circ}C^{-1}$ (up to 300° C) and $17.4 \times 10^{-6}\,^{\circ}C^{-1}$ (up to 500° C) [11]. The thermal expansion coefficient of 45S5 glass and 39.6 vol% dense 100 μm fibre compacts were measured* to be

$$\alpha_g = 18.0 \times 10^{-6}\,^{\circ}C^{-1} \text{ (up to 450° C)}$$

$$\alpha_{\text{porous metal}} = 20.0 \times 10^{-6}\,^{\circ}C^{-1} \text{ (up to 200° C)}$$

$$21.8 \times 10^{-6}\,^{\circ}C^{-1} \text{ (up to 400° C).}$$

Measuring the thermal expansion coefficient of dense stainless steel yielded the values given in the literature.

The difference between thermal expansion coefficients of dense and porous stainless steel arises for the following reason.

When the sintered porous metal specimen is heated, tensile stresses are developed in the fibres since there are multiple sinter bonds between fibres. The fibres would normally retain their original kinked shapes if they were not multiply linked to neighbouring fibres, but, because of the geometrical constraints imposed by this, they cannot. The tensile stresses so developed tend to straighten the fibres in a manner which is just the reverse of the kinking of slender bars described by the Euler theory. The net result of expansion of the metallic fibres and their straightening is a thermal expansion coefficient comparatively larger than that obtained for dense metal. Upon cooling down, the fibres tend to regain their original size and shape, independent of whether the pores have been filled with glass or not. Therefore it is appropriate to use the thermal expansion coefficient of the sintered porous fibre structure to describe the residual stress pattern in the composite after immersion.

It follows from the measured values that $\Delta\alpha_c = \alpha_g - \alpha_f < 0$ and thus that compressive residual stresses are created in the glass matrix.

The complete filling of the pores depends on the viscosity of the glass. which in turn is altered by variations of the temperature and the composition of the glass melt. While it was not appropriate to change the glass composition for considerations of thermal expansion and biocompatibility, the glass temperature could be controlled easily with increments of 10° C. Alterations of glass melt temperature, and thus viscosity, to control the thickness of the glass rim outside the composite structure were not sought in the present study. It was, however, observed that at 1375° C, which is the maximum allowable temperature due to Na-volatization at greater temperatures, all types of sintered specimens were infiltrated.

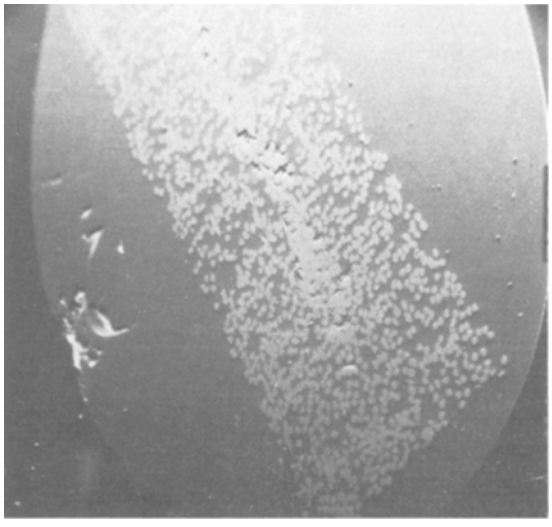

Figure 5 Micrograph of a longitudinal section of the composite, showing the crack free outer glass rim and the presence of some mid-line flaws.

There must be a lower limit of pore size in the sintered fibre preform below which glass cannot flow into the porous compact. Apparently this limit was not reached in the present experiments. Specimens of six different pore geometries were made by using three fibre diameters (50, 100 and 200 μm) and two different volume percentages of fibres (45 and 60%). Specimens made with 60 vol% fibres of 50 μm diameter, and thus the smallest mean pore size, were still completely filled with glass. Using small fibres with higher fibre to glass ratios was not meaningful for reasons of mechanical strength, as is discussed in a later section.

The presence of entrapped gases generally prevented the glass from impregnating all the pores in the centre of the compact leading to an array of flaws in the middle of the specimens. Vacuum impregnation could probably eliminate this source of heterogeneity. Fig. 5 is a micrograph of a polished cross-section of a specimen with 45 vol% 50 μm diameter fibres, showing the array of mid-line flaws. The higher fibre content is an artifact due to closure of unfilled pores during

*Measurements were taken using an Orton dilatometer with 50.8 mm long by 6.35 diameter cylindrical specimens.

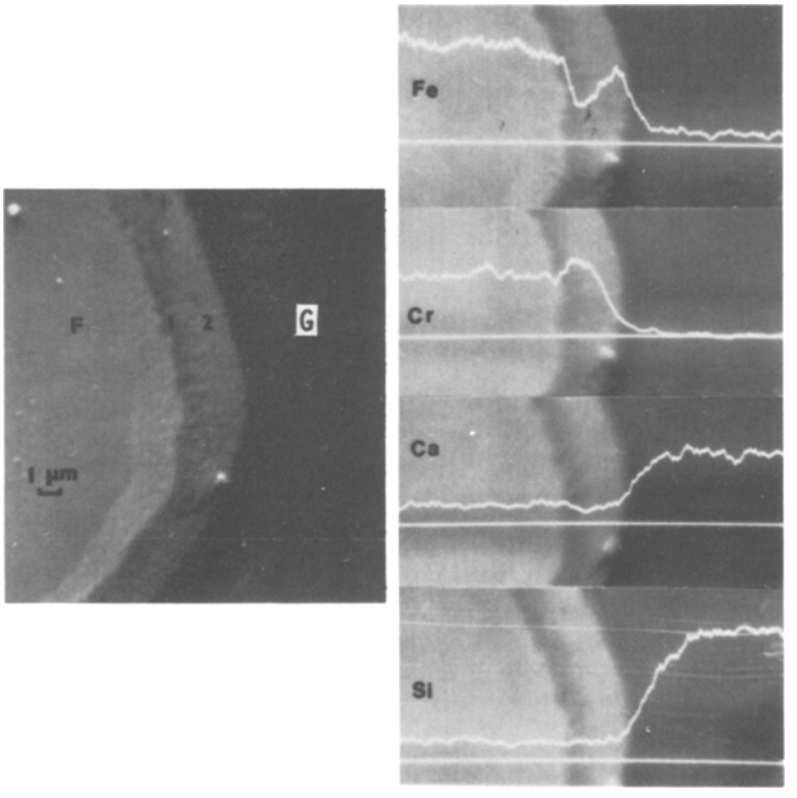

Figure 6 Interfacial chemical analysis of the fibre to glass bond.

grinding and polishing. This figure also clearly shows the outer glass rim free of cracks and the intimate intermixture of glass and metal fibres.

In order to promote the formation of a physical bond between glass and metal fibres, and not just a mechanical intertwining, the metal compact was oxidized in air at 800° C for ten minutes prior to immersion. An oxide interface, typically 5 μm thick was obtained. Electron microprobe analysis (EMP) as well as scanning electron microscopy (SEM) with energy dispersive X-ray analysis (EDXA) indicated the existence of a dual oxide layer (see Fig. 6). A chromium-rich oxide which is depleted in Fe is formed on the metal fibre; a second layer in contact with glass contains Fe in an amount comparable to the bulk composition, but has a very limited amount of Cr. In the glass a gradient of Si from the bulk to the oxide layer can be observed.

Following the oxidation heat treatment, a short (20 min) thermal hold at a lower temperature (400° C) was necessary for the 50 μm fibre composite in order to control total metal expansion during immersion in the 1350 to 1380° C molten glass. This additional step was not necessary for the 100 μm fibre compact because the larger diameter fibres did not expand so rapidly in the short (3 to 4 sec) immersion in the molten glass. The consequence of not controlling this variable for the 50 μm fibre structures was cracking in the glass rim and at times in the matrix which could not be eliminated by post-immersion annealing. After control of the above variables, a final anneal for 4 h at 400 to 500° C followed by a slow furnace cool was used to ensure relief of excessive stresses in the glass rim.

6. Mechanical testing results

Tensile tests were made on a series of composites fabricated with 50, 100 and 200 μm fibres, moulded to different vol% fibres in the range 40 to 60%. All compacts in this first series were sintered at 1250° C; for 2 hours for the 50 μm fibre preforms, and for 4 hours for the 100 and 200 μm fibres structures. A fibre shrinkage conditioning treatment of 20 min at 400° C was used for all specimens of the first series, i.e., 7 specimens for each different composite.

After establishing tendencies from the first series, the two best preform microstructures were selected for more detailed investigation using 3-point as well as tensile tests and three different

TABLE I results of the first series of tensile tests (mean values and standard deviation, SD). For comparison purposes the mechanical properties of the parent glass [12] and the porous fibre material [13] are also included

Sample*	Sample type	$\sigma_{0.01}$ (MPa)	SD	UTS (MPa)	SD	E (GPa)	SD
50-S-45	Bioglass–steel	59	5	80	17	112	13
50-S-60	composite	45	3	81	9	83	4
100-S-45		49	12	55	7	98	10
100-S-60		55	2	97	11	107	8
200-S-60		40	2	54	9	108	18
50-S-45	Porous fibre	20		70-110		35	
50-S-60	metal	42		140		65	
100-S-45		10		70		20	
100-S-60		30		135		65	
Bioglass 45-S-5	Parent glass			42			

*Sample name is composed as follows; 1st figure represents the fibre diameter in μm, S represents stainless steel, and the second figure represents vol% of fibres.

surface finishes. The second series compares 50-S-45 specimens (50 μm fibres at 45 vol%) with 100-S-60 specimens (100 μm fibres at 60 vol%). In this second series, only the 50-S-45 specimens were subjected to the metal fibre shrinkage conditioning treatment.

Before all tests the excess outer glass rim was removed by sand blasting and subsequent grinding on consecutive SiC grits up to 320 (first series) or 80, 320 or 600 (second series).

The results of the first series are represented in Table I together with the properties of the parent glass [12] and the porous fibre material [13]. They show that an increase of volume per cent of the 50 μm fibres causes a decrease of yield strength, while the ultimate strength (UTS) remains unchanged; the modulus of elasticity also goes down (mean value for 50-S-45 is 112 GPa and for 50-S-60 is 83 GPa). The latter observation is in apparent contradiction with any theoretical assessment of the modulus of elasticity of composites, which projects a larger modulus for an increasing fraction of the higher modulus constituent. Considering also that the yield strength of the parent porous material and the A-50-S-60 composite is essentially the same (42 to 45 MPa), these observations fit a pattern suggesting that the distance between neighbouring fibres has become too small to have a strengthening effect on the glass. In such a case, it is essentially the properties of the metal phase of the composite that are measured. The compressive stress fields of neighbouring fibres probably interfere with each other to such an extent that no appreciable strengthening can be achieved.

Specimens made of 100 and 200 μm diameter fibres with respective fibre contents of 45 and 60 vol% had a substantially lower ultimate tensile strength than other series of specimens. Moreover, the 100-S-45 series showed a very limited elongation to failure.

On the basis of these results, the second series of tensile and three-point bend tests were limited to composites made either of 45 vol% 50 μm (50-S-45) and 60 vol% 100 μm fibres (100-S-60).

The results of the second series of tensile testing are compiled in Table II. The final grinding grit, and thus surface finish, has no appreciable effect within these series. It was therefore considered justified to collect all data for each type of

TABLE II Mean values and standard deviation (SD) of yield stress and ultimate tensile strength, measured in tension; five values were used per mean, except where indicated between brackets

Composite type	Surface finish	$\sigma_{0.01}$ (MPa)	SD	$\sigma_{0.2}$ (MPa)	SD	UTS (MPa)	SD
50-S-45	Grit 80	57.5 (6)	10.6	79.0	13.2	94.8	20.2
	Grit 320	67.1	13.6	78.6	9.4	89.6	9.6
	Grit 600	64.4	15.5	84.5	6.9	100.8	7.8
100-S-60	Grit 80	55.6 (6)	10.0	72.0	5.1	95.6	13.0
	Grit 320	58.3	10.7	76.2	11.3	96.2	11.4
	Grit 600	59.9	10.2	72.7	8.3	103.2	17.8

TABLE III Mean strength values and standard deviation (SD) of two composites, as measured by tensile and three-point bend testing

Sample	Mode of testing	$\sigma_{0,01}$ (MPa)	SD	$\sigma_{0.2}$ (MPa)	SD	UTS (MPa)	SD
50-S-45	Tension*	61.9	11.8	78.3	11.2	91.9	15.2
	Bending†	-		167.6	38.4	290.4	42.4
100-S-60	Tension*	57.0	8.6	73.3	7.1	97.9	12.8
	Bending†	-		162.9	31.4	339.9	71.9

*Twenty specimens.
†Ten specimens.

specimen in order to compare larger sets of tensile data with three-point bend data, as is done in Table III. Comparison of results of the same composites between the two series indicate the reproducibility of the mechanical properties.

A considerable difference in ultimate tensile strength is noted between the results obtained by tensile testing and by 3-point bend testing (Table III). This difference is attributed to the nature of the tests and to the distribution of microstructural flaws in the glass. In tensile testing, specimens fail in the weakest section, since stresses are uniform along the length of the specimens. In three-point bending the highest stresses are generated under the load, which is not necessarily the weakest section. In addition, bending tests generally yield higher tensile strengths than tensile tests, depending upon the value of the Weibull modulus [14]. Also, the flaws present at the centre of the specimens of these series will predominantly influence the ultimate tensile strength in tension, but not in bending: indeed, normal stresses are uniform across the cross-section in tension, but are nil at the neutral axis, and thus at the flaws, in bending.

These results show the marked increase of strength of the composite over the bulk glass due to the reinforcement of the ductile metal wires. Comparing the parent glass strength as measured in diametral compression (Table I: 42 MPa) and the strength in bending of the composite a considerable reinforcement has occured. The strength values of the composites are close to the upper bound value which can be assumed by

$$\sigma_c = \sigma_{fu} V_f + \sigma_{mu} V_{mu}, \quad (2)$$

where σ_c is the composite strength, σ_{fu} is the ultimate fibre strength, V_f is the fibre volume-fraction, σ_{mu} is the ultimate matrix strength and V_{mu} is the matrix volume-fraction, is valid within the assumptions of continuous reinforcement of aligned fibres, equal strains in both components and absence of internal stresses [8]. With $\sigma_{fu} =$ 530 MPa and $\sigma_{mu} = 42$ MPa, the composite strengths given in Table IV are obtained.

However, since internal compressive stresses are present, and since the matrix stress, σ_{mu}, is probably larger as the glass is strained as a micrometre sized beam in between fibres, the actual strength effect by just adding two materials together should be lower than the calculated numbers would indicate: there is thus still room for increasing the strength.

This can probably be brought about by further optimization of the fibre diameter, the respective fractions of both constituents and the fibre to glass bonding.

7. Ductility and fractographic analysis

The present composites display a marked ductility. In tension testing up to 10% deformation to failure is reproducibly observed. In three-point bend testing plastic deformation until a bending angle of over 90° is invariably obtained; this was the maximum attainable with the experimental set-up used (see Fig. 7).

Fig. 3, a recorded tensile graph, clearly shows the onset of plastic deformation, the strain hardening and the continuous deformation after the ultimate tensile strength has been reached. Specimens tested in tension until 0.1% plastic deformation did not show any microstructural damage in the glass. Onset of plastic deformation of the composite is thus probably by plastic deformation of the metal fibres. Subsequently, however, multiple cracking of the matrix occurs. Fracto-

TABLE IV Calculated and measured composite strengths for two optimized microstructures

Composite	Composite strength (MPa)	
	Calculated	Measured
50-S-45	262	290
100-S-60	335	335

These calculated values are very close to the measured values.

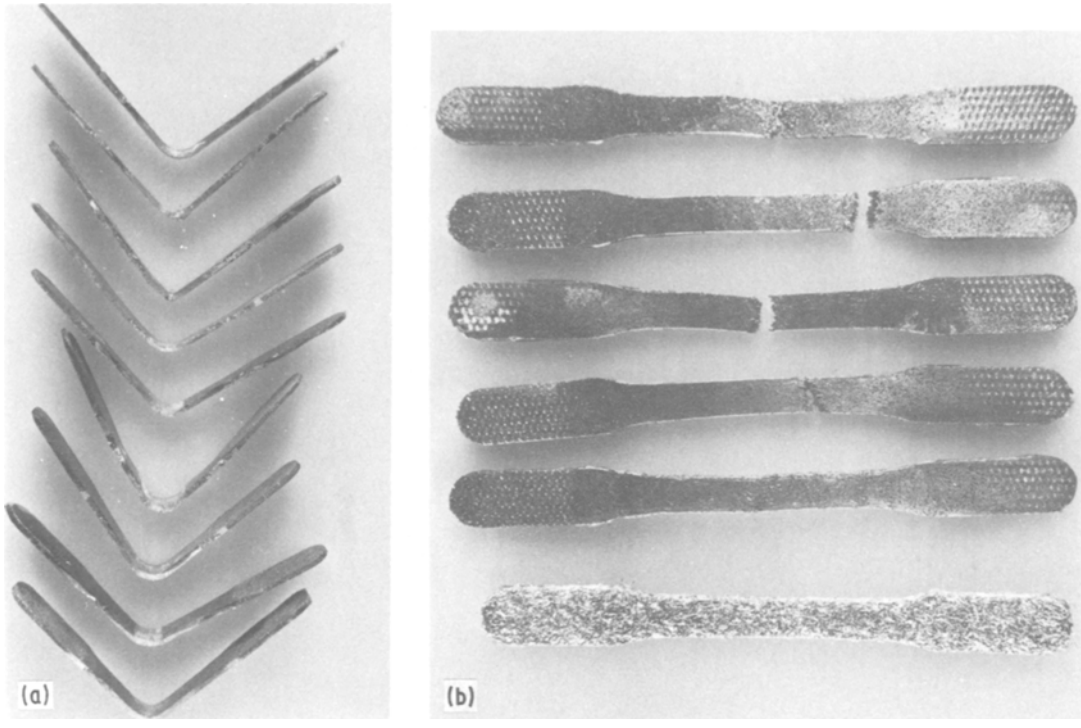

Figure 7 Series of mechanically tested specimens, (a) 50-S-45 specimens tested in 3-point bending and (b) 100-S-60 specimens tested in tension.

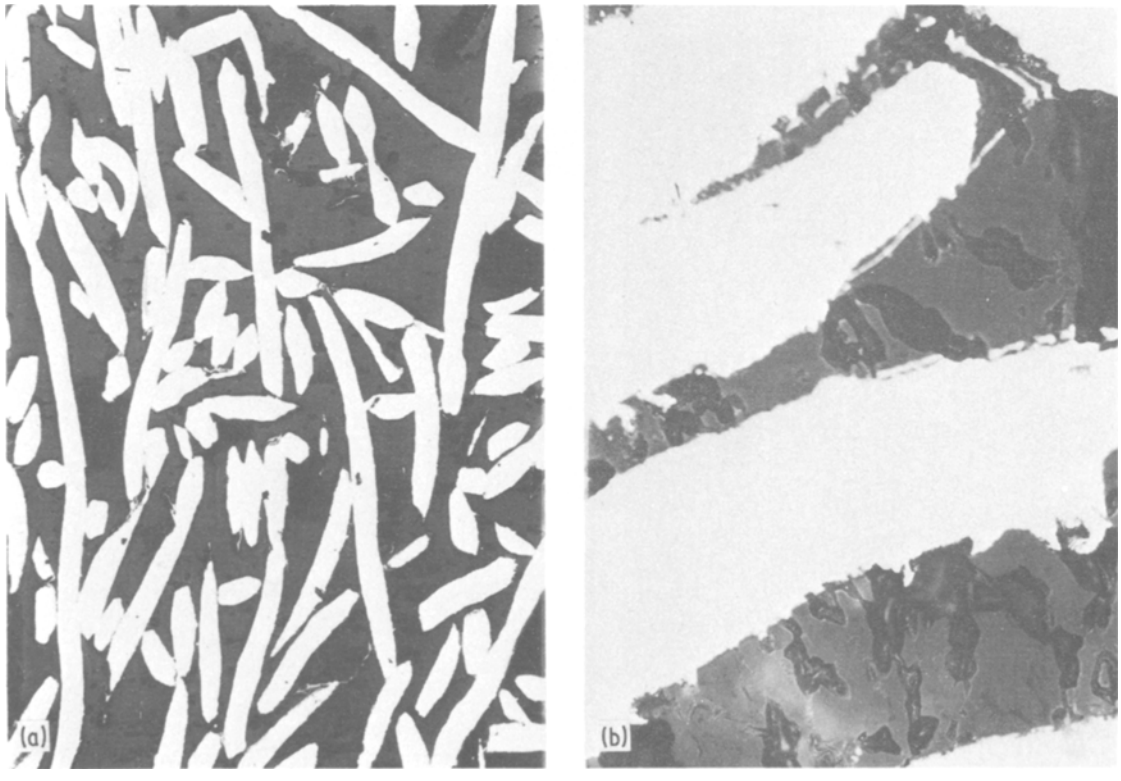

Figure 8 Longitudinal section of a 50-S-45 specimen (a) remote from the fracture surface and (b) close to the fracture surface. Note the difference in extent of structural damage, the orientation of cracks perpendicular to the tensile direction and the crack blunting at the fibres.

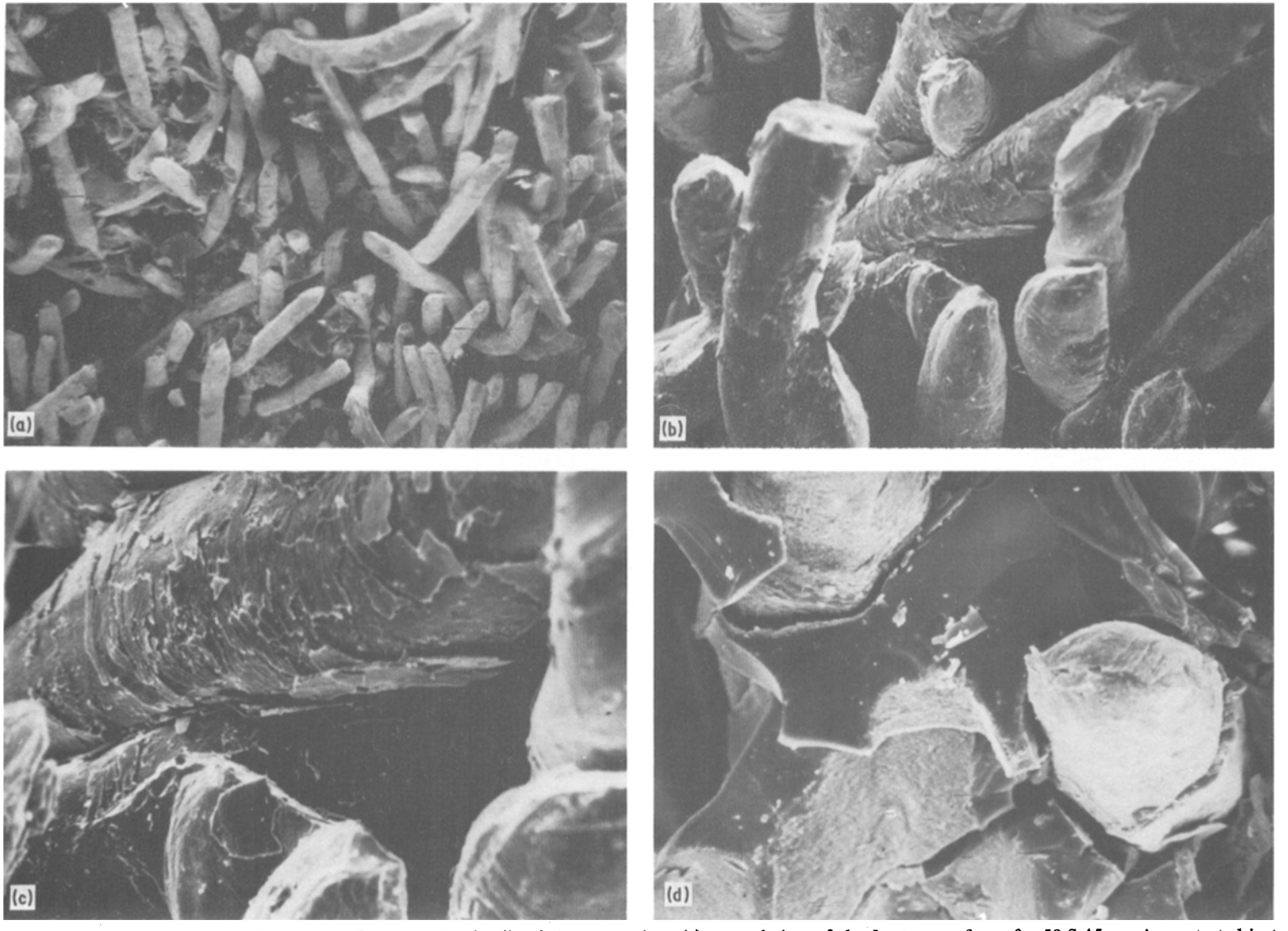

Figure 9 Scanning electron micrograph, showing fractographic details of the composites, (a) general view of the fracture surface of a 50-S-45 specimen, tested in tension (b) ruptured fibres and a pulled-out fibre in the fracture surface of the same specimen (c) detail of oxide scaling-off upon ultimate deformation; there is no more fibre-glass bonding (d) glass remant in the centre portion of the photograph.

graphic analysis shows cracks in the glass, perpendicular to the tensile direction, with blunting of the cracks by the fibres. Cracking is extensive at the fracture surface, but is more limited away from it (see Fig. 8). There is no debonding between fibre and glass except at the fracture surface and its immediate vicinity. This indicates that stress transfer between fibre and glass remains good until structural damage is close to yielding complete failure of the composite. Only then does debonding and fibre pull-out take place.

Scanning electron microscopical examination reveals that the extensive elongation at the fracture surface is almost solely due to the stretching and pull-out of the fibres from the glass matrix: there is little glass in between the fibres and it is the fibres that are torn and not their sinter-bonds. The stretched fibres elongate without the glass, after debonding between glass and fibre occurred. Only at spots where the cracking was perpendicular to the fibre does the glass remain on the fibre (see Fig. 9). These observations suggest that:

(a) There is an effective compromise in the bioglass–stainless steel composites between the contradictory requirements of strength and toughness. Best strength is reached for a high interfacial bond between constituents, but fibre pull-out adds considerably to toughness [8]. The present composite fulfills the requirements set for both properties; e.g. initially good interfacial bonding is achieved, giving high strength, but fibre pull-out eventually occurs causing a large expenditure of deformational energy.

(b) The present composites are materials where the high toughness is the sum of two different mechanisms, plastic deformation of the fibres and fibre pull-out.

(c) There is a five-step failure pattern for the composite: (1) failure is initiated by cracking of the glass perpendicular to the tensile stresssing direction; (2) the cracks are blunted by the presence of the fibres; (3) the fibres are plastically deformed; (4) fibres and glass debond, and (5) the metal fibres are ruptured.

Since these failure steps are additive a large increase in failure stress is obtained for the composite bioglass.

8. Conclusions

The results reported here lead to the following conclusions:

(a) Immersion is a simple and effective method for preparing metal fibre reinforced bioglass composites.

(b) The sintering of the stainless-steel porous skeleton is essential for the subsequent glass impregnation to be effective.

(c) The microstructure of the porous stainless steel skeleton has a major effect on the properties of the composite. Combinations of 45 vol% of 50 μm fibres or 60 vol% of 100 μm fibres produce both high strength and large strains to failure.

(d) Metal fibre reinforcement effectively transforms bioglass into a structurally reliable material. Both strength and toughness are markedly superior to the properties of the parent bioglass. This dual improvement is due to residual compressive stresses in the glass matrix (because the metal has a higher thermal expansion coefficient than the glass), a higher modulus of elasticity of the fibres and effective stress transfer between fibres and glass.

(e) The plastic deformation required for reliable performance of many surgical devices can be achieved with the bioglass–stainless steel composite without ultimate failure.

Acknowledgements

The present work was financially supported in part by NATO Research Grant Number 1582. The metal fibres used in this study were kindly provided by NV Bekaert, Zwevegem, Bergium. The laboratory assistance of W. Lacefield is gratefully acknowledged.

References

1. L. L. HENCH and H. A. PASCHALL, *J. Biomed. Mater. Res. Symp.* **4** (1973) 25.
2. A. E. CLARK Jr, L. L. HENCH and H. A. PASCHALL, *J. Biomed. Mater. Res.* **10** (1976) 161.
3. B. A. BLENCKE, J. BROEMER and K. K. DEUTSCHER, *ibid.* **12** (1978) 307.
4. J. WILSON, G. H. PIGGOT, F. J. SCHOEN and L. L. HENCH, *ibid,* in press.
5. J. WILSON, G. MERWIN and L. L. HENCH, unpublished work.
6. D. C. GREENSPAN and L. L. HENCH, *J. Biomed. Mater. Res. Symp.* 7 (1976) 503.
7. P. BUSCEMI and L. L. HENCH, in "An Investigation of Bonding Mechanisms of the Interface of a Prosthetic Material", U.S. Army Medical Research and Development Command Contract DAMD 17-76-C-6033, Report no. 7, 55-61 (1976).
8. I. W. DONALD and P. W. McMILLAN, *J. Mater. Sci.* **11** (1976) 949.
9. E. D. CLARK, Proceedings of the Conference on Advanced Materials and Composites, Cocoa Beach,

Florida. January 1977.
10. B. A. BOLEY and J. H. WEINER, "Theory of Thermal Stresses", (John Wiley Inc., New York, (1960).
11. "Metals Handbook" 8th edn. (American Society for Metals, Metals Park, Ohio, 1967) p. 422.
12. L. G. HOUSEFIELD, MSc thesis, University of Florida (1972).
13. P. DUCHEYNE, E. AERNOUDT and P. DE
14. F. F. LANGE, in "Annual Review of Materials Science" edited by R. A. Huggins, R. H. Bube and R. W. Roberts (Annual Reviews Inc., Palo Alto, California, 1974) p. 365.

Received 27 April
and accepted 23 July 1981